Energy-Efficient Resource Allocation for Fractional Frequency Reuse in Heterogeneous Networks

Kemal Davaslioglu, *Student Member, IEEE*, Cemil Can Coskun, *Student Member, IEEE*, and Ender Ayanoglu, *Fellow, IEEE*

***Abstract*—Next generation wireless networks face the challenge of increasing energy consumption while satisfying the unprecedented increase in the data rate demand. To address this problem, we propose a utility-based energy-efficient resource allocation algorithm for the downlink transmissions in heterogeneous networks (HetNets). We consider the fractional frequency reuse (FFR) method in order to mitigate the intra- and inter-cell interference. The proposed algorithm divides the resource allocation problem into frequency and power assignment problems and sequentially solves them. The proposed power control algorithm uses the gradient ascent method to control the transmit power of macrocell base stations (MeNBs) as most of the power in the network is consumed there. We present the optimality conditions of the resource allocation problem and the convergence of the proposed algorithm. In order to mitigate the inter-cell interference further, we study the interference pricing mechanisms and obtain an upper bound to the maximum energy efficiency problem including the inter-cell interference contributions. The performance of the proposed algorithm is studied in a Long Term Evolution (LTE) system. Our simulation results demonstrate that the proposed algorithm provides substantial improvements in the energy efficiency and throughput of the network. It is also shown that interference pricing provides only marginal improvements over the proposed algorithm.**

***Index Terms*—Energy efficiency, heterogeneous cellular networks, power control, pricing, long term evolution.**

I. Introduction

ENERGY efficiency is an important issue in the next generation wireless networks. In particular, the high data rate demands of the LTE standards bring the hidden cost of increasing energy consumption. These have been studied in the literature under the topic of "Green Communications" [1]. Network operators are also seeking green solutions in order to reduce their operational expenses. Several methods have been investigated and standardized to increase the energy efficiency of the networks, see, e.g., [1]–[5]. Among these solutions, we study the FFR method in this paper to reduce both the intra- and inter-cell interference. In the FFR method, cells are divided into cell-center and cell-edge regions and orthogonal subbands are allocated in these regions. In an interference dominated region, increasing the transmit power slightly improves the throughput, but it significantly degrades the energy efficiency. The frequency allocation of the FFR method significantly increases the energy efficiency and reduces the outages.

The resource allocation problem for multicell networks has been widely investigated in the literature, see, e.g.,[6]–[10]. Reference [6] investigates resource allocation in time, frequency, and both time and frequency domains. In [7], a heuristic algorithm, which minimizes the duality gap, is presented to solve the sum rate maximization problem using constant energy allocation across subbands. Considering the complexity of the problem and practical constraints, both references [6] and [7] propose to use constant energy allocation across subbands instead of using a multi-user water-filling algorithm. It needs to be noted that the same constraints also apply to the LTE systems, where the standards define the smallest scheduling granularity to be per resource block (RB) and constant power is allocated to the subcarriers within an RB [2]. In this paper, we also employ this approach and find the optimal power levels that maximize the energy efficiency of the network. Recently, several studies have been reported investigating energy-efficient resource allocation in multicell networks, see, e.g., [8]–[10]. These works consider static power consumption along with transmit power to develop better link adaptation schemes. In our paper, this problem is also addressed but in a large scale such that the energy efficiency of the network is maximized considering the static and dynamic power consumption at MeNBs.

The FFR scheme has been studied extensively in the context of Orthogonal Frequency Division Multiple Access (OFDMA) systems, see, e.g., [11]–[16]. The capacity and coverage characteristics of various FFR schemes are analytically investigated in [11] using stochastic geometry methods. Similar to our paper, the study in [11] also uses constant power allocation across subbands. However, the FFR scheme employed in [11] is prone to high cross-tier interference for small cells, especially those close to the MeNB, as they are not protected from the MeNB downlink transmissions. In FFR schemes, the system performance closely depends on the cell-center region radius. Reference [12] investigates the dependence of optimal cell-center radius on the number of users. It identifies that as the number of users increases, the optimal cell-center radius needs to decrease. The study in [13] finds that the network sum throughput is maximized when the radius of the cell-center region is chosen as 0.6 times the cell radius for single-layer networks, employing omnidirectional antennas. A similar study

Manuscript received July 18, 2014; revised December 23, 2014 and April 15, 2015; accepted May 24, 2015. Date of publication June 1, 2015; date of current version October 8, 2015. This work was partially supported by the National Science Foundation under Grant No. 1307551. Any opinions, findings, and conclusions or recommendations expressed in this material are those of the authors and do not necessarily reflect the view of the National Science Foundation. The associate editor coordinating the review of this paper and approving it for publication was L. Song.

The authors are with the Center for Pervasive Communications and Computing, Department of Electrical Engineering and Computer Science, University of California, Irvine, CA 92697-2625 USA (e-mail: kdavasli@uci.edu).

Color versions of one or more of the figures in this paper are available online at http://ieeexplore.ieee.org.

Digital Object Identifier 10.1109/TWC.2015.2438826

is presented in [14] for two-layer networks with three and six sector antennas in which 0.61 and 0.54 times the cell radius, respectively, are determined to be the cell-center region radii that maximize the network throughput. In contrast to the studies in [13], [14] which consider only the network throughput, in this paper, we also investigate the cell-center radius that maximizes the energy efficiency. This subject has not been investigated in the literature. Recent studies in [14]–[16] propose a novel FFR scheme for multi-tier HetNet deployments with sectorized MeNBs. In this paper, we employ the same FFR scheme. Also, our paper differs from [11]–[16] in that power control across subbands is employed to optimize the system performance in terms of energy efficiency.

In this paper, we address the resource allocation problem in OFDMA systems employing the FFR method in HetNets deployments. We propose a novel resource allocation algorithm in which the objective is to maximize the energy efficiency in each sector. We account for both the transmit and static power consumed at base stations. The proposed algorithm divides the resource allocation problem into frequency and power allocation problems. To solve the frequency assignment problem, we investigate two well-known schedulers, the sum rate maximization (SRM) and equal bandwidth (EBW) schedulers, see, e.g., [17]. For power control assignments, the gradient ascent method is applied. We note that power control is applied only at the MeNB and not at the picocell base station (pico eNB). The reasons that power control is not applied at the pico eNBs are twofold. First, the maximum power transmission of pico eNBs ensures full coverage is provided in the small cells. Second, the backhaul congestion can be avoided as the network becomes denser with small cell deployments and excessive traffic overhead can be eliminated. The proposed framework can be considered as a non-cooperative resource allocation in which only the intra-cell interference information is required.

In dense urban scenarios with overlapping base station coverage, however, the inter-cell interference may become a critical factor. In such scenarios, non-cooperative resource allocation does not account for the loss in utility one causes to other users due to interference. This is called as negative externality in economics [18]. One of the mechanisms that addresses this problem is to employ the interference pricing method. We study this method to provide an upper bound to the preceding framework in terms of energy efficiency and account for the negative externalities in the power allocation step. In interference pricing, downlink transmissions of base stations are penalized based on the inter-cell interference that they create. In general, this topic is investigated under the game-theoretic pricing research area in the literature, see, e.g., [18]–[23]. In [18]–[20], the authors study a linear pricing function and propose an asynchronous distributed pricing (ADP) algorithm for ad-hoc networks. The pricing function reflects the marginal change in the utility per unit interference. Each terminal announces an interference price and then updates its power. The bottleneck of the ADP algorithm is that each terminal requires the interference price information of all other users, which is often difficult to distribute in practice. The authors of [18]–[20] also show that the solution satisfies the Karush-Kuhn-Tucker (KKT) conditions. Note that the power control problem in multicell networks is a non-convex problem which means that it can have multiple local optima and the KKT conditions can only guarantee local optimality. However, in general, convergence to the global optimal point is difficult to achieve. In our paper, we applied the ADP approach to our algorithm in order to obtain an upper bound to its performance. Through simulations, we demonstrated that pricing brings only marginal improvements. This shows that the proposed algorithm reaches close to the optimal performance while requiring only intra-cell information exchange.

The remainder of the paper is organized as follows. Section II introduces the system model and presents the base station power consumption models. Section III formulates the energy-efficient resource allocation in LTE systems employing FFR method. The algorithm is proposed in Section III, along with implementation steps, optimality conditions, and convergence proof. Section IV introduces the pricing methods that consider inter-cell interference in the resource allocation. Numerical results are presented in Section V and concluding remarks are made in Section VI.

II. System Model

In this section, we first present the FFR method used in this paper. Then we identify the interference conditions in each region and present the system model. Finally we discuss the base station power consumption models that are used to derive energy-efficient algorithms.

Interference is a key problem in mobile wireless communication systems. In today's mobile communication networks, base station distances are typically on the order of less than a kilometer for urban deployments. This poses a challenging interference problem for HetNet deployments due to the large downlink transmit power differences. For example, the MeNBs and pico eNBs differ by 16 dB in their transmit power levels [2]. In order to mitigate interference, several methods have been proposed such as FFR [14], enhanced inter-cell interference cancellation [2], coordinated multipoint transmissions [24], and carrier aggregation [2]. In the FFR method, different subbands are allocated in different regions. Each cell is divided into two regions as the cell-center and cell-edge region. Depending on the locations, the macrocell and picocell associated users, abbreviated as MUEs and PUEs, respectively, are assigned to different subbands. This orthogonal frequency assignment significantly reduces both the intra- and inter-cell interference. In this paper, we denote the cell-center region radius as r_{th}. This distance sets the region boundaries. For example, users that are closer than r_{th} to the MeNB are considered to be in the cell-center and those that are farther are considered to be in the cell-edge. Similarly, users connected to a pico eNB located closer than r_{th} to the MeNB are considered to be in the cell-center.

Consider the FFR scheme depicted in Fig. 1, which is designed for the MeNBs employing three sector antennas with the objective of mitigating the interference. The system bandwidth is partitioned into four subbands. Subband A is assigned to the cell-center region for the macrocell tier, and the rest of the spectrum is divided into three subbands, one subband for each sector is used in the macrocell cell-edge for the MUEs, as shown

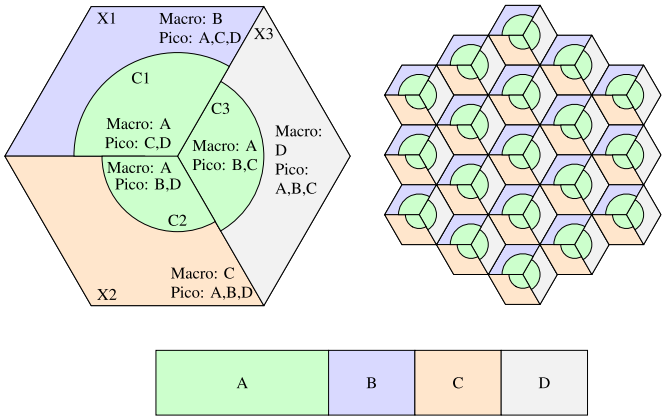

Fig. 1. Illustration of spectrum allocations in a multi-tier FFR network with dynamic cell-center region boundaries in which the MeNBs employ three sector antennas, whereas pico eNBs have omnidirectional antennas. Note that the picocell coverage areas are not depicted in the figure.

in Fig. 1. This allocation means that frequency reuse (FR) of three is used in the macrocell tier for the cell-edge. Since the inter-cell interference is mitigated, the outages at the cell-edge MUEs are reduced. In the picocell tier, two of the remaining subbands are allocated to the PUEs in the cell-center region, while subband A and the same two subbands are used in the cell-edge region. With the pico eNBs in cell-edge region using the rest of the subbands, better use of spectrum resources can be achieved. Due to different spectrum allocations, interference conditions vary depending on the cell region and the associated tier. Let us identify the interference conditions for the MUEs and PUEs in the cell-center and cell-edge regions in different sectors. For example, in Sector 1, the MUEs in the cell-center region are assigned to subband A, while the PUEs in the same region are allocated to subbands C and D. On the other hand, in the cell-edge region, the MUEs are scheduled on subband B, whereas the PUEs operate on subbands A, C, and D.

First, consider the MUEs in the cell-center region that are scheduled on subband A. The strongest interfering base stations for the users in this region are the six MeNBs in the first ring surrounding this cell. Also, note that the surrounding 12 MeNBs in the second ring create interference although at smaller magnitudes. As for the cross-tier interference, the cell-edge pico eNBs transmiting on subband A create interference for these users. Then, we can express the signal-to-interference-plus-noise ratio (SINR) of a cell-center MUE k on subcarrier n as

$$\gamma_k^{(n)} = \frac{P_M^{(n)} g_{k,b}^{(n)}}{\sum\limits_{b' \in \mathcal{B}_M^A, b' \neq b} P_M^{(n)} g_{k,b'}^{(n)} + \sum\limits_{b'' \in \mathcal{B}_P^A} P_P^{(n)} g_{k,b''}^{(n)} + N_0 \Delta_f} \quad (1)$$

where $P_M^{(n)}$ and $P_P^{(n)}$ denote the downlink transmit powers of macrocell M and picocell P on subcarrier n, respectively. The channel gain between user k and base station b is denoted by $g_{k,b}^{(n)}$ on subcarrier n. Also, $\mathcal{B}_M^A$ and $\mathcal{B}_P^A$ denote the set of MeNBs and pico eNBs operating on subband A. The thermal noise power per Hz is denoted by N_0. The bandwidth of a subcarrier is represented as Δ_f, $\Delta_f = 15$ kHz for LTE systems [2]. It is straightforward to derive the interference conditions for the cell-center MUEs in Sectors 2 and 3, and these are omitted due to space considerations. The SINR of the MUEs in the cell-edge regions can be obtained similarly. In this region, the number of interfering MeNBs in the first ring is reduced from six to two due to the frequency reuse of 1/3. This comes from the sectorization at the MeNBs. As in the cell-center region, the picocells operating on subband B still interfere with the cell-edge MUEs. The five MeNBs in the second ring also create interference, but relatively less compared to those from the first tier.

Let us now discuss the interference conditions for the PUEs. Assume that a PUE k is located in the cell-center region of Sector 1. This user can be scheduled on the resources over the subbands C and D. The interference from the picocell tier comes from the pico eNBs operating over these subbands. These correspond to the pico eNBs within the same cell and those in the neighboring cells. The interference from the macrocell tier is mainly caused by the four MeNBs in the first ring, in which each MeNB creates interference for either one of these subbands. Note that the closest MeNB does not interfere with the pico eNBs in the cell-center region as they are allocated to different subbands. Hence, this spectrum allocation significantly decreases the number of interfering MeNBs for the picocell tier, and thereby reduces the cross-tier interference. The SINR of a PUE in the cell-center region scheduled to the subcarriers in subband C is

$$\gamma_k^{(n)} = \frac{P_P^{(n)} g_{k,b}^{(n)}}{\sum\limits_{b' \in \mathcal{B}_M^C} P_M^{(n)} g_{k,b'}^{(n)} + \sum\limits_{b'' \in \mathcal{B}_P^C, b'' \neq b} P_P^{(n)} g_{k,b''}^{(n)} + N_0 \Delta_f} \quad (2)$$

where $\mathcal{B}_M^C$ and $\mathcal{B}_P^C$ denote the set of MeNBs and pico eNBs operating on subband C. Similar expressions can be obtained for the other PUEs, in which the only differences will be the interfering base stations.

Constant power allocation over subbands is considered in this paper, which follows the standards for LTE systems [12]. The proposed algorithm in Section III-A introduces two power control parameters β and ε to adjust the downlink transmit power levels. The first parameter β scales the transmit power of each MeNB. The second parameter ε denotes the ratio of the power allocated to the subcarriers in the cell-edge region to those in the cell-center region. By this way, ε characterizes the fairness between the MUEs in the cell-center and cell-edge regions. Let N_A, N_B, N_C, and N_D denote the total number of subcarriers in subbands A, B, C, and D, respectively. Then, for Sector 1, the maximum transmit power of an MeNB satisfies

$$\beta P_{\max,M} = P_M N_A + \varepsilon P_M N_B, \quad (3)$$

and therefore, $P_M = \beta P_{\max,M}/(N_A + \varepsilon N_B)$, where P_M and $P_{\max,M}$ are the MeNB transmit power per subcarrier in the cell-center region and the MeNB maximum transmit power, respectively. The term εP_M denotes the transmit power per subcarrier for the MUEs in the cell-edge region. Similar expressions can be obtained for Sectors 2 and 3 by replacing N_B with N_C and N_D, respectively. For completeness, we also express the picocell

transmit power per subcarrier. For a pico eNB in Sector 1, the transmit power per subcarrier, denoted by P_P, depends on the picocell's location in the cell, and it is given by

$$P_P = \begin{cases} P_{\max,P}/(N_C + N_D) & \text{if } d_p \le r_{th} \\ P_{\max,P}/(N_A + N_C + N_D) & \text{if } d_p > r_{th} \end{cases} \quad (4)$$

where P_P and $P_{\max,P}$ are the transmit power of a pico eNB per subcarrier and the maximum transmit power of a pico eNB, respectively. The distance between the closest MeNB and pico eNB is denoted by d_p. Similar expressions can be obtained for Sectors 2 and 3.

A. Base Station Power Consumption Models

Recent studies have quantified the energy consumption of a base station down to the component level and several power consumption models have been proposed, see, e.g., [25]–[27]. These models include the contributions of the power amplifier, radio frequency (RF) transceiver parts, baseband unit, power supply, and cooling devices [25]. Using these models each component's contribution can be identified and efficient methods can be developed to introduce energy savings [1]. In this paper, we study the load-dependent power consumption model presented in [25], which is

$$P_{Total} = \begin{cases} N_{TRX}(P_0 + \Delta \cdot P_{TX}) & 0 < P_{TX} \le P_{\max} \\ N_{TRX}P_{sleep} & P_{TX} = 0 \end{cases} \quad (5)$$

where P_{Total} and P_{TX} are the overall base station power consumption and RF transmit output powers, respectively. N_{TRX} is the number of transceiver chains, P_0 is the power consumption at the minimum non-zero output power, and Δ is the slope of the load-dependent power consumption. P_{sleep} denotes the power consumption of the sleep mode. Notice that the power consumption at a base station depends on the RF transmit power, P_{TX}, and thereby this model is referred to as load-dependent power consumption model. Using this definition, the power consumption at an MeNB and a pico eNB can be expressed as

$$\begin{aligned} P_{Macro} &= N_{TRX,M}(P_{0,M} + \Delta_M P_{TX,M}) \\ P_{Pico} &= N_{TRX,P}(P_{0,P} + \Delta_P P_{TX,P}) \end{aligned} \quad (6)$$

where $P_{0,M}$, $P_{0,P}$, P_{Macro}, and P_{Pico} are the power consumption at the minimum non-zero output power and the total power consumption of the MeNBs and pico eNBs, respectively. $N_{TRX,M}$ and $N_{TRX,P}$ represent the number of transceiver chains at the MeNBs and pico eNBs, respectively. The corresponding slopes of the load-dependent power consumption are denoted as Δ_M and Δ_P, in the same order as before. Note that (6) is true for $0 < P_{TX,M} \le P_{\max,M}$ and $0 < P_{TX,P} \le P_{\max,P}$, where $P_{\max,M}$ and $P_{\max,P}$ are the maximum RF transmit power for MeNBs and pico eNBs, respectively. If $P_{TX,M} = 0$ (or $P_{TX,P} = 0$), then $P_{Macro} = N_{TRX,M}P_{sleep,M}$ (or $P_{Pico} = N_{TRX,P}P_{sleep,P}$), where $P_{sleep,M}$ and $P_{sleep,P}$ are the power consumption of the sleep modes of MeNBs and pico eNBs, respectively. Table I presents the corresponding parameter values of the linearized power consumption model for various base station types.

TABLE I
BASE STATION POWER CONSUMPTION MODEL PARAMETER VALUES [25]

Base Station Type	P_0 (W)	P_{sleep} (W)	$P_{\max}$ (W)	Δ
MeNB	130	75.0	20	4.7
Pico eNB	56	39.0	6.3	2.6

III. ENERGY-EFFICIENT RESOURCE ALLOCATION PROBLEM

In this section, we formulate a non-cooperative resource allocation problem in OFDM systems employing the FFR method. Our objective is to maximize the energy efficiency per sector by determining the optimal RB allocation and power level assignment on each subband. In the sequel, we define the energy efficiency per sector, formulate the problem, and present its complexity analysis. Then, we proceed to propose our algorithm, along with its complexity analysis, optimality conditions, and convergence analysis.

Let $R_k(\gamma_k)$ denote the throughput of user k that depends on its SINR γ_k. Also, let $\mathcal{K}^C_{M,i}$, $\mathcal{K}^X_{M,i}$, $\mathcal{K}^C_{P,i}$, and $\mathcal{K}^X_{P,i}$ denote the set of MUEs in sector i connected to the MeNB in the cell-center and cell-edge regions, and the set of PUEs connected to the pico eNBs in the cell-center and cell-edge regions of this sector, respectively. Note that the subscript i denotes the sector indices. Then, the energy efficiency per sector i is given by

$$\eta_{EE,i} = \frac{\sum\limits_{k \in \mathcal{K}^C_{M,i} \cup \mathcal{K}^X_{M,i}} R_k(\gamma_k) + \sum\limits_{k \in \mathcal{K}^C_{P,i} \cup \mathcal{K}^X_{P,i}} R_k(\gamma_k)}{\psi_i} \quad (7)$$

where the total power consumed per sector i is denoted by ψ_i which can be expressed as

$$\begin{aligned} \psi_i = {} & N_{TRX,M,i}(P_{0,M} + \Delta_M P_{TX,M}) \\ & + N_{\text{picos}} N_{TRX,P,i}(P_{0,P} + \Delta_P P_{TX,P}) \end{aligned} \quad (8)$$

and where N_{picos} is the number of pico eNBs in sector. The energy efficiency is given in units of bits/Joule.

The energy-efficient resource allocation problem can be formulated as

$$\max_{\mathbf{F},\mathbf{P}_M,\mathbf{P}_P} \ \eta_{EE,i} \quad (9)$$

where $\mathbf{F}$ denotes the RB allocation vector, and $\mathbf{P}_M$ and $\mathbf{P}_P$ are the MeNB and pico eNB power assignment vectors. The solution requires a joint search over the frequency and power domains. It is shown in [6] that the optimal solution is the multilevel water-filling solution. However, finding the optimal RB assignments among K users and N_{RB} RBs requires $K^{N_{RB}}$ searches [6]. Therefore, this approach is impractical for real applications and it can lead to large latencies in practice as there are more users in the system. In the next subsection, we present our proposed algorithm that divides the resource allocation

problem into two stages decoupling the frequency and power allocation problems.

A. Proposed Solution

Obtaining the instantaneous interference conditions of the complete network is often impractical for real applications due to excessive traffic overhead it would require. Therefore, recent studies have focused on non-cooperative or clustered base station resource allocation algorithms in multicell systems, see, e.g., [8], [9], and Chapter 11 of [2]. In this paper, we investigate a non-cooperative solution in which each MeNB sector maximizes its own energy efficiency. We assume that there is a fast and reliable information exchange between the MeNB and the pico eNBs in the same sector such that the channel conditions of the PUEs are known at the MeNB. In LTE, this is exchanged over the X2 interface [2].

The proposed algorithm starts with determining cell-center region boundaries. We compare two different algorithms for this purpose, one of which maximizes the energy efficiency, while the other ensures a fair distribution of resources which is presented here as a reference. Then, we decouple the frequency and power allocation problems into two stages. In the first stage, we solve the frequency assignment problem. Once these are obtained, in the second stage, we assign the power levels that maximize the energy efficiency at each sector.

1) Setting The Cell-Center Region Boundaries: The cell-center region radius per sector, r_{th}, is an important design parameter that affects the system performance in OFDMA systems employing the FFR method. It determines the set of MUEs in the cell-center and cell-edge regions. We assume that MeNBs have perfect knowledge about the locations of pico eNBs. Once the cell-center radius is determined, it is easy to identify the pico eNBs in each region. Considering the spatial and temporal variations of the user distribution in each cell, this parameter needs to be dynamically adjusted per sector. We propose an algorithm to determine the cell-center region boundaries and compare its performance to another algorithm where the frequency resources are distributed proportionally among the users in the same sector.

In the first algorithm, the MUE with the highest reference signal received power (RSRP) measurement, that is typically the closest MUE to the MeNB, is selected to be in the cell-center region, while the rest of the MUEs are in the cell-edge region. The SINR of this user is, in general, expected to be greater than the other MUEs. Consequently, the cell-center region subbands are allocated to only one MUE maximizing its throughput. In general, this algorithm achieves the maximum throughput and energy efficiency at the cost of system fairness. We refer to this algorithm as Adaptive R_{th} Algorithm 1.

In the second algorithm, the cell-center region boundary is determined such that the ratio of cell-center and cell-edge MUEs is proportional to the ratio of the subbands allocated in these regions. First, the MUEs are sorted in ascending order based on their path losses. Let N_M^C and N_M^X denote the number of subcarriers that the MeNB uses in the cell-center and cell-edge regions. For K MUEs in sector i, we round $(N_M^C/(N_M^C + N_M^X) \cdot K)$ to the nearest integer, and $\lfloor 0.5 + N_M^C/(N_M^C + N_M^X) \cdot K \rfloor$ users are considered in the cell-center region. The rest of the users are assigned to the cell-edge subbands. This achieves higher fairness, but this comes at the cost of a decrease in the sector throughput. We refer to this algorithm as Adaptive R_{th} Algorithm 2. Note that a similar method is proposed in [28] to determine the cell-center boundaries.

In terms of implementation, MUEs are differentiated as cell-center and cell-edge users using the RSRP measurements. If the RSRP of a user is higher than a threshold, the user is considered to be in the cell-center region. Alternatively, the reference signal received quality (RSRQ) measurements can also be used depending on the system design. Especially, when the shadow fading effects are significant, the RSRQ measurements, which can be considered as the wideband SINR, can provide a better correlation with the user-experienced SINR. On the other hand, it is shown in [29] that both schemes perform almost the same. In this paper, we employ the RSRP measurements to determine cell-center and cell-edge users due to simplicity. For example, with the Adaptive R_{th} Algorithm 1, the user with the highest RSRP is determined to be in the cell-center.

2) Frequency Assignment Problem: In order to solve the frequency assignment problem we study two schedulers. First, we study the SRM scheduler discussed in [17]. In this scheduler, the RBs are assigned to users such that the throughput is maximized. This scheduler is investigated to maximize the throughput, although this comes at the cost of a decrease in the system fairness. The second scheduler we study is the EBW scheduler. Consider K users sharing N_{RB} RBs. Then, $K_h = \text{mod}(N_{RB}, K)$ users get $\lfloor N_{RB}/K \rfloor + 1$ RBs, whereas $K_i = K - K_h$ users are given $\lfloor N_{RB}/K \rfloor$ RBs. Although the EBW scheduler does not necessarily maximize the energy efficiency per sector, it is proposed in [30] to calibrate system level simulations. This scheduler serves as a point of reference to a fair distribution of resources, which is used to quantify the scheduling gain in Section V. Note that although these two schedulers are commonly studied in the literature, they do not guarantee satisfaction of the QoS constraints of every user. These constraints can be addressed in the resource allocation problem using QoS-aware schedulers, see, e.g., [4]. In QoS-aware schedulers, the multi-user frequency assignments are carried out to satisfy constraints such as the user's guaranteed bit rate requirement, packet error rate of different data traffic classes, latency, etc.

3) Power Assignment Problem: The second stage of the proposed algorithm solves the power control problem by assigning the optimal power levels to the subbands. The proposed algorithm uses the gradient ascent method to solve this problem. First we observe that by controlling the transmissions for the cell-center MUEs, we also determine how much interference is created for the cell-edge PUEs. Similarly, the downlink transmissions for the cell-edge MUEs determine the interference for the cell-center PUEs. In order to capture these two effects, we introduce two variables into the optimization problem as β and ε, as discussed in Section II.

Consider the following function $\eta_i(\varepsilon, \beta)$ that only includes the throughput of users in sector i who are affected by the optimization variables ε and β. Those users are the MUEs in both regions and the PUEs in the cell-edge region. While

calculating $\eta_i(\varepsilon, \beta)$ only the interference created within each sector is considered. The energy efficiency function in sector i can be modified as

$$\eta_i(\varepsilon, \beta) = \frac{\sum_{k\in\mathcal{K}^C_{M,i}} R_k(\gamma_k) + \sum_{k\in\mathcal{K}^X_{M,i}} R_k(\gamma_k) + \sum_{k\in\mathcal{K}^X_{P,i}} R_k(\gamma_k)}{\psi_i} \quad (10)$$

where the power consumed in sector i is denoted by ψ_i. We modify (8) to account for the power control parameter β such that ψ_i can be expressed as

$$\psi_i = N_{TRX,M,i}(P_{0,M} + \Delta_M \beta P_{\max,M}) + N_{\text{picos}} N_{TRX,P,i}(P_{0,P} + \Delta_P P_{\max,P}). \quad (11)$$

Hence, β can be used to introduce energy savings in the total RF transmit power.

The energy efficiency per sector definition in (10) can be expanded as

$$\eta_i(\varepsilon, \beta) = \frac{\Delta f \sum_{k\in\mathcal{K}^C_{M,i}} \sum_{n\in\mathcal{N}^C_{M_k}} \log_2\left(1 + \frac{\beta P_{\max,M} g^{(n)}_{k,m}}{(N^C_M + \varepsilon N^X_M) I^{(n)}_k}\right)}{\psi_i} + \frac{\Delta f \sum_{k\in\mathcal{K}^X_{M,i}} \sum_{n\in\mathcal{N}^X_{M_k}} \log_2\left(1 + \frac{\beta\varepsilon P_{\max,M} g^{(n)}_{k,m}}{(N^C_M + \varepsilon N^X_M) N_0 \Delta_f}\right)}{\psi_i} + \frac{\Delta f \sum_{k\in\mathcal{K}^X_{P,i}} \sum_{n\in\mathcal{N}^X_{P_k}\cap\mathcal{N}^C_M} \log_2\left(1 + \frac{P_{\max,P}\frac{g^{(n)}_{k,p}}{N^X_P}}{\frac{\beta P_{\max,M} g^{(n)}_{k,M}}{N^C_M + \varepsilon N^X_M} + N_0\Delta_f}\right)}{\psi_i} \quad (12)$$

where $I^{(n)}_k$ is the interference from the picocells using subband A in cell-edge region plus the thermal noise effective over a subcarrier at the PUE. The expression $n \in \mathcal{N}^X_{P_k} \cap \mathcal{N}^C_M$ in (12) denotes the subcarriers that the downlink transmissions of the cell-center MUEs creates interference for the cell-edge PUEs, which are the subcarriers in subband A for the FFR scheme in Fig. 1. It needs to be emphasized that (12) considers only the intra-cell interference and not the inter-cell interference. This enables fast implementation as it does not necessitate information exchange between MeNBs and asynchronous implementation at each MeNB sector. For that reason, this type of formulation is robust against inter-cell backhaul transmission delays.

The optimization problem that maximizes the energy efficiency per sector can be written as

$$\max_{\varepsilon,\beta} \quad \eta_i(\varepsilon, \beta) \qquad \text{s.t.} \quad \varepsilon \geq 1 \text{ and } 0 \leq \beta \leq 1. \quad (13)$$

The first constraint is to favor the MUEs in the cell-edge region such that they are transmitted at least ε times the power allocated for the MUEs in the cell-center region. This parameter also affects the interference incurred at the cell-edge PUEs. The second constraint scales the total RF transmit power of the MeNB and sets the boundary conditions. Hence, the variable β not only determines the interference, but it also introduces energy savings to the system.

B. Optimality Conditions

The Lagrangian of the problem in (13) can be written as

$$\mathcal{L}(\varepsilon, \beta, \boldsymbol{\lambda}) = \eta_i(\varepsilon, \beta) + \lambda_1(\varepsilon - 1) + \lambda_2\beta + \lambda_3(1 - \beta) \quad (14)$$

where λ_1, λ_2, and λ_3 are the Lagrange multipliers and $\boldsymbol{\lambda} = (\lambda_1, \lambda_2, \lambda_3)$. Note that if (ε^*, β^*) solves (13), then $\eta_i(\varepsilon^*, \beta^*) \geq \eta_i(\varepsilon, \beta)$ for all $\epsilon \geq 1$ and $0 \leq \beta \leq 1$. Furthermore, there exists $\boldsymbol{\lambda}^* \geq 0$ such that the following optimality conditions are satisfied

$$\frac{\partial\mathcal{L}(\varepsilon^*, \beta^*, \boldsymbol{\lambda}^*)}{\partial\varepsilon} = \frac{\partial\eta_i(\varepsilon^*, \beta^*)}{\partial\varepsilon} + \lambda^*_1 = 0,$$
$$\frac{\partial\mathcal{L}(\varepsilon^*, \beta^*, \boldsymbol{\lambda}^*)}{\partial\beta} = \frac{\partial\eta_i(\varepsilon^*, \beta^*)}{\partial\beta} + \lambda^*_2 - \lambda^*_3 = 0, \quad (15)$$

and the complementary slackness conditions are

$$\lambda^*_1(\varepsilon^* - 1) = 0, \qquad \lambda^*_2\beta^* = 0,$$
$$\lambda^*_3(1 - \beta^*) = 0, \qquad \lambda^*_1, \lambda^*_2, \lambda^*_3 \geq 0. \quad (16)$$

The equations in (15)–(16) are commonly known as the KKT conditions [31]. It needs to be emphasized that the power control parameters ε and β depend on the number of RBs allocated to the cell-center and cell-edge regions, the channel conditions, the maximum transmit powers, and the bandwidth of each subcarrier.

C. Gradient Ascent Method

The gradient ascent method starts at an initial (ε, β) value evaluated at time t and the parameters ε and β are updated

$$\varepsilon_{t+1} = \varepsilon_t + \mu_t \nabla_\varepsilon \eta_i(\varepsilon_t, \beta_t)$$
$$\beta_{t+1} = \beta_t + \mu_t \nabla_\beta \eta_i(\varepsilon_t, \beta_t) \quad (17)$$

where ε_{t+1} and β_{t+1} are the updated values at time $t+1$, respectively. $\nabla_\varepsilon\eta_i(\varepsilon, \beta) = \partial\eta_i(\varepsilon, \beta)/\partial\varepsilon$ and $\nabla_\beta\eta_i(\varepsilon, \beta) = \partial\eta_i(\varepsilon, \beta)/\partial\beta$ are the partial derivatives of η_i with respect to ε and β, respectively, evaluated at time t. These partial derivatives are multiplied by a sufficiently small and positive step size μ_t. The step size at each iteration is chosen according to the Armijo rule [31]. In this rule, the step size is chosen as $\mu_t = \mu_0^m s$, where s is a constant and m is the first non-negative integer that satisfies the following inequality

$$\eta_i(\varepsilon_{t+1}, \beta_{t+1}) - \eta_i(\varepsilon_t, \beta_t) \geq \rho\mu_t \nabla\boldsymbol{\eta}_i(\varepsilon_t, \beta_t)^T \mathbf{d}_t \quad (18)$$

where ρ is a fixed constant and $\mathbf{d}_t$ is a feasible direction. The gradient is shown by $\nabla\boldsymbol{\eta}_i(\varepsilon, \beta) = [\nabla_\varepsilon\eta_i(\varepsilon, \beta)\nabla_\beta\eta_i(\varepsilon, \beta)]^T$, where $[\cdot]^T$ denotes the transpose operator. Starting from $m = 0$, it is successively increased until (18) is satisfied. Note that the gradient ascent method without the Armijo rule can fail

to converge to a stationary point as illustrated in [31, p. 26], but when the step size is determined with the Armijo rule, it is guaranteed that the energy efficiency per sector increases per iteration until the algorithm converges. This enables selecting the increment that sufficiently improves the current objective value. Typical values of these constants are such that $\rho \in [10^{-5}, 10^{-1}]$ and $\mu_0 \in [0.1, 0.5]$ [31]. The directional vector $\mathbf{d}_t$ is an ascent direction if it satisfies $\nabla \boldsymbol{\eta}_i(\varepsilon_t, \beta_t)^T \mathbf{d}_t > 0$ if $\nabla \boldsymbol{\eta}_i(\varepsilon_t, \beta_t) \neq \mathbf{0}$, and $\nabla \boldsymbol{\eta}_i(\varepsilon_t, \beta_t)^T \mathbf{d}_t = 0$ if $\nabla \boldsymbol{\eta}_i(\varepsilon_t, \beta_t) = \mathbf{0}$. In this paper, we consider the steepest descent method, that is $\mathbf{d}_t = \nabla \boldsymbol{\eta}_i(\varepsilon_t, \beta_t)^T$. The expressions of the partial derivatives $\nabla_\varepsilon \eta_i(\varepsilon, \beta)$ and $\nabla_\beta \eta_i(\varepsilon, \beta)$ can be found in the Appendix.

D. Convergence Analysis

In what follows, we investigate the convergence of the proposed algorithm. To this end, we first show the quasiconcavity of the objective function η_i with respect to the optimization variables ε and β. Then, we study the optimality of the solutions obtained by the gradient ascent method.

Definition 1: A function f is called quasiconcave if its domain, denoted by $\operatorname{dom} f$, is convex and for any $x, y \in \operatorname{dom} f$,

$$f(\phi x + (1-\phi)y) \geq \min\{f(x), f(y)\} \tag{19}$$

where $0 \leq \phi \leq 1$ [32]. Similarly, a function f is called strictly quasiconcave if it satisfies (19) with strict inequality for $x \neq y$ and $0 < \phi < 1$ [32].

Proposition 1 (First-Order Characterization): Let $f(\mathbf{x})$ be a continuously differentiable function on an open and convex set $\mathcal{D} \subset \mathbb{R}^n$. Then, f is quasiconcave if and only if $f(\mathbf{y}) \geq f(\mathbf{x})$ implies $\nabla f(\mathbf{x})^T(\mathbf{y} - \mathbf{x}) \geq 0$, for all $\mathbf{x}, \mathbf{y} \in \mathcal{D}$ [32].

Proposition 2 (Second-Order Characterization): Let $f(\mathbf{x})$ be a twice differentiable function and its dimensions be denoted by n. If $f(\mathbf{x})$ is quasiconcave, then $\mathbf{y}^T \nabla^2 f(\mathbf{x}) \mathbf{y} \leq 0$ holds for all $\mathbf{x} \in \operatorname{dom} f$ and $\mathbf{y} \in \mathbb{R}^n$ satisfying $\mathbf{y}^T \nabla f(\mathbf{x}) = 0$ [32].

Lemma 1: Let $\mathcal{D}$ be a nonempty convex set and f be a strictly quasiconcave function. Then, any local maximum is a global solution of the problem $P = \sup\{f(x) | x \in \mathcal{D}\}$ [32].

A proof of Lemma 1 can be found in [32]. In cases where the concavity (or similarly convexity) of the problem cannot be assumed, the results of Lemma 1 are important to determine global extreme points. In fact, these are directly applicable to problems in several research fields such as those in economics. We refer the reader to Appendix C.6 of [32] for an example problem in economics, the standard consumer demand problem in a deterministic framework. It needs to be emphasized that care needs to be taken in applying Lemma 1. The local extreme point of a quasiconcave (or quasiconvex) problem should not be confused with the stationary points as for determining the global extreme point. Next, using the definitions and lemmas above, we present Lemma 2, whose proof is provided in the Appendix due to its length.

Lemma 2: The energy efficiency per sector expression η_i is strictly quasiconcave in ε and β.

Theorem 1: The proposed update rules for ε and β in (17) converge to the global optimal solution of the problem (13) as $t \to \infty$ for a sufficiently small step size μ_t.

Proof: It follows from Lemma 1 that if there exists a local solution to the maximization problem, then there is a global maximum. It is straightforward to show that the gradient ascent method with sufficiently small step sizes converges to the globally maximum solution. □

IV. Energy-Efficient Resource Allocation With Pricing

In this section, we extend the preceding energy-efficient resource allocation and introduce pricing methods to achieve an upper bound to the non-cooperative energy efficiency maximization problem. Pricing methods are shown to be efficient in wireless communications [18]–[23]. In particular, we investigate the ADP framework and employ the interference pricing function. This function is motivated by the fact that without the penalty functions, base stations act selfish and transmit without any inter-cell interference concerns. When the pricing schemes are introduced, resources can be more efficiently shared among selfish players and the inter-cell interference can be reduced so that a better overall solution can be achieved. Consider that an MeNB i solves the following maximization problem

$$\begin{aligned} \max_{\varepsilon,\beta} \quad & \eta_i(\varepsilon, \beta) - \theta_i(\varepsilon, \beta) \\ \text{s.t.} \quad & \varepsilon \geq 1 \text{ and } 0 \leq \beta \leq 1. \end{aligned} \tag{20}$$

where the energy efficiency function, $\eta_i(\varepsilon, \beta)$, is penalized with the interference pricing cost function, $\theta_i(\varepsilon, \beta)$. This problem has the same boundary constraints as in (13). Depending on the system design, various penalty functions can be defined, see the survey in [23]. In this paper, we take the inter-cell interference into consideration. The interference pricing function is defined as [18]–[20]

$$\theta_i(\varepsilon, \beta) = \sum_{n \in \mathcal{N}_M} p_k^{(n)} \sum_{j \in \mathcal{K}^{(n)}, j \neq k} \pi_j^{(n)} g_{i,j}^{(n)} \tag{21}$$

where $\mathcal{N}_M$ denotes set of subcarriers used in the cell-center and cell-edge regions, that is $\mathcal{N}_M^C \cup \mathcal{N}_M^X \subseteq \mathcal{N}_M$. The transmit power of an MeNB i to user k on subcarrier n is represented by $p_k^{(n)}$, i.e., P_M on the subcarriers used in the cell-center region and εP_M for those in the cell-edge region. The set of users assigned to subcarrier n in the system is denoted by $\mathcal{K}^{(n)}$ and the notation $j \in \mathcal{K}^{(n)}, j \neq k$ denotes any user that MeNB i interferes on subcarrier n. The interference caused by MeNB i to user j on subcarrier n is denoted by $g_{i,j}^{(n)}$. The interference prices are given by $\pi_j^{(n)} = -\partial u_j^{(n)}(\gamma_j^{(n)}) / \partial I_j^{(n)}$, where $u_j^{(n)}(\gamma_j^{(n)})$ and $I_j^{(n)}$ denote the utility and the incurred interference of user j on subcarrier n, respectively. The KKT conditions of the problem in (20) are similar to those in (15), (16) except for the interference terms of each user also includes the inter-cell interference. Due to space considerations, these conditions are not repeated here. Note that using the results in [18]–[20], it can be shown that the solution of the problem in (20) is guaranteed to converge to a point which satisfies the KKT conditions, although global optimality is not guaranteed. Despite the fact that interference pricing can be implemented in an asynchronous and distributive manner, it requires each base station to acquire the interference prices of

all the other base stations on all subcarriers. This means that, based on the FFR scheme in Fig. 1, 57 ($N_M^C + N_M^X$) prices need to be distributed at each subframe through the backhaul, which is hard to implement in practice. Therefore, this is presented as an upper bound for energy efficiency in the non-cooperative energy efficiency maximization problem without pricing. Note that in terms of implementation, the pricing algorithm requires both the intra-cell and inter-cell information exchange among base stations, whereas the proposed algorithm without pricing only necessitates the intra-cell information. Both of these can be conveyed through the X2 interface for LTE systems.

V. Numerical Results

In this section, the performance of the proposed algorithm is evaluated. We quantify the individual contributions of power control, frequency scheduling, cell-center region radius, spectrum allocation, and pricing. We compare the performance of the proposed algorithm to the orthogonal and cochannel spectrum allocation, and demonstrate the achievable gains. In addition, we investigate three algorithms for determining the cell-center region boundaries. We investigate the Adaptive R_{th} Algorithms 1 and 2, described in Section III-A. Also, we consider the case with the fixed FFR boundaries, in which the cell radius that maximizes the average energy efficiency is chosen through enumeration methods. Note that this analysis is presented in Fig. 5(a) and (b). Based on this analysis, we find that when the cell-center region radius is taken as 0.3 times the cell radius, it maximizes the average energy efficiency. In terms of spectrum allocation, MeNBs and pico eNBs transmit over all subcarriers in the cochannel allocation, whereas the spectrum is divided into 32 and 18 non-overlapping RBs for the MeNBs and pico eNBs, respectively, in the orthogonal channel allocation. For the FFR method, there are 32 RBs in the subband *A* and 6 RBs are allocated to subbands *B*, *C*, and *D* [13]. The same spectrum allocation is employed for the no power control FFR algorithm case, abbreviated as No PC in Figs. 3 and 4. We compare our proposed algorithm with different power control algorithms and spectrum allocations. In particular, we compare the proposed algorithm with the power control algorithms proposed in [7] and [14], and spectrum allocation schemes of cochannel, orthogonal channel, and FR schemes. First, we have implemented the constant power allocation algorithm proposed in [7] using the FFR scheme in Fig. 1. This algorithm maximizes the sector sum rate and achieves the smallest duality gap. However, as we will demonstrate shortly, it does not perform well in an interference dominated multicell environment. Second, we evaluate the performance of the algorithm proposed in [14] which employs the power control parameters as $(\varepsilon, \beta) = (4, 1)$ and the FFR scheme in Fig. 1. For different spectrum allocation schemes, we implement the cochannel and orthogonal frequency allocation in which base stations transmit at maximum power. To demonstrate the gain of FFR over FR spectrum allocation, we have also implemented the FR scheme using the proposed power control algorithm. In the FR scheme, the system bandwidth is divided into three subbands in which each MeNB sector uses one of the three subbands, while the remaining two subbands are allocated to the picocell tier.

TABLE II
Simulation Parameters

Parameter	Setting
Channel bandwidth	10 MHz
Total number of data RBs	50 RBs
Freq. selective channel model (CM)	Extended Typical Urban CM
UE to MeNB PL model	$128.1 + 37.6 \log_{10}(d)$
UE to pico eNB PL model	$140.7 + 36.7 \log_{10}(d)$
Effective thermal noise power, N_0	-174 dBm/Hz
UE noise figures	9 dB
MeNB and Pico eNB antenna gain	14 dBi and 5 dBi
UE antenna gain	0 dBi
Antenna horizontal pattern, $A(\theta)$	$-\min(12(\theta/\theta_{3\text{dB}})^2, A_m)$
A_m and $\theta_{3\text{dB}}$	20 dB and 70°
Penetration loss	20 dB
Macro- and picocell shadowing	8 dB and 10 dB
Inter-site distance	500 m
Minimum macro- to user distance	50 m
Minimum pico- to user distance	10 m
Minimum pico- to macro- distance	75 m
Minimum pico- to pico- distance	40 m
Traffic model	Full buffer

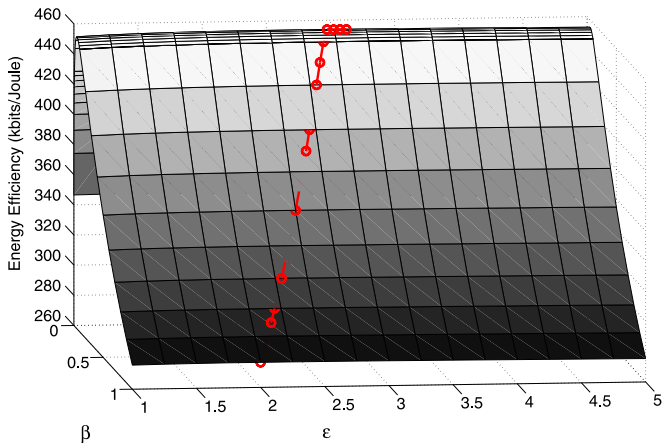

Fig. 2. Illustration of the energy efficiency of a sector and the proposed algorithm solutions using the gradient ascent method.

The simulation layout is shown in Fig. 1. It assumes a HetNet deployment with 19 hexagonal cells in which MeNBs are employed with 3-sector antennas. In each sector, there is a single antenna, i.e., $N_{TRX,M,i} = 1, \forall i$. For the pico eNBs, omnidirectional antennas are employed, i.e., $N_{TRX,P,i} = 1, \forall i$. There are 4 randomly placed pico eNBs in each sector. In order to observe the clustering effects, we consider nonuniform user distribution and generate 30 users per sector. First, we place one user per pico eNB within a 40 meter radius, while the rest of the users are randomly generated within the sector area. The users are associated to the base stations with the highest reference signal received power (RSRP) method [33]. While generating the pico eNBs and users, several minimum distance constraints are considered and these are presented in Table II, along with the other parameters and simulation models used in our numerical results. These parameters and channel models are in accordance with [30] for the baseline simulation of HetNets. Also, we consider $\rho = 10^{-2}$ and $\mu_0 = 0.05$ for the gradient ascent method.

Fig. 2 illustrates the energy efficiency of a sector for different (ε, β) pairs. The improvement of the proposed algorithm at each iteration is denoted by the red circles. Armijo rule is

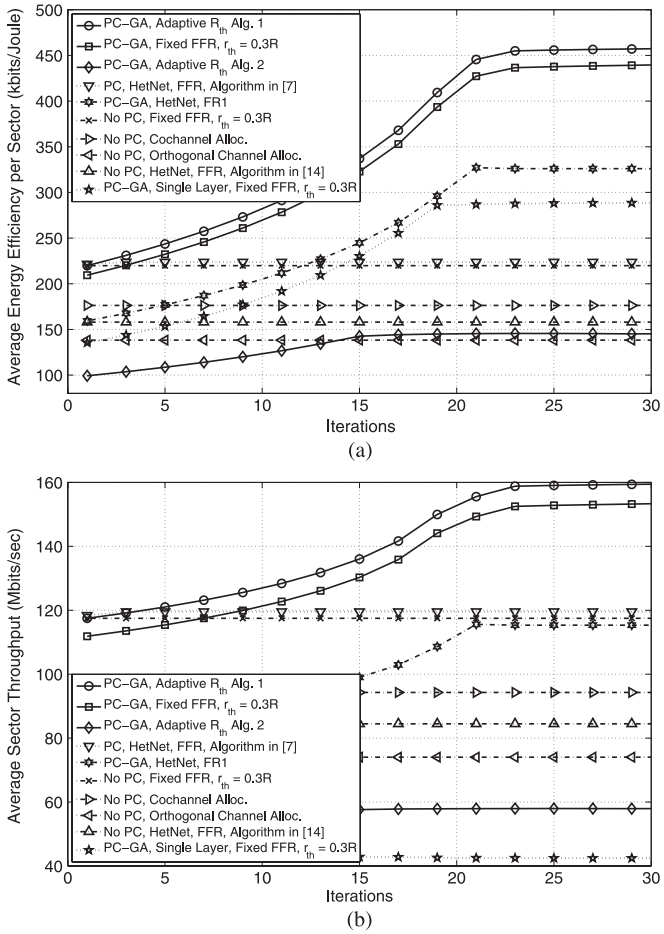

Fig. 3. Average energy efficiency per sector (a) and average sector throughput. (b) are depicted for the EBW scheduler.

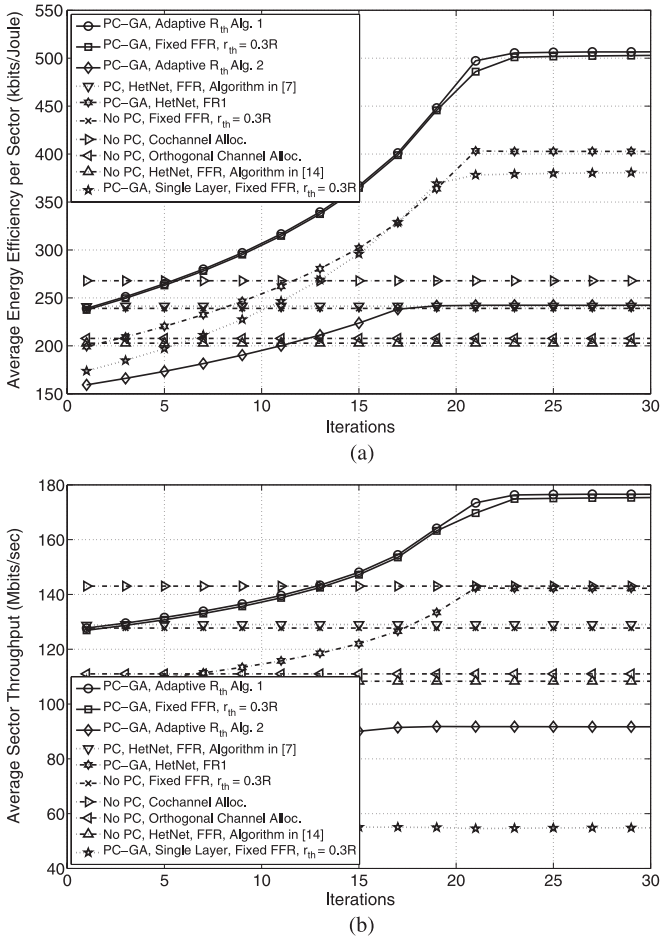

Fig. 4. Average energy efficiency per sector (a) and average sector throughput (b) are depicted for the SRM scheduler.

implemented to select the step sizes. As studied in Section III-A, this rule guarantees that energy efficiency increases at every iteration until it converges. Fig. 2 shows that the energy efficiency of the network is mostly affected by β. On the other hand, the effects of ε on energy efficiency are minor for the same β. This is expected since β determines the macrocell transmit power level which directly affects the total consumed power in the network, whereas ε does not change the total consumed power, but its effects are mostly observed on the total throughput.

In Figs. 3(a), (b) and 4(a), (b), we investigate the individual contributions of the methods to determine the cell-center boundaries, frequency scheduling, and power control gains for different schedulers. In Fig. 3(a) and (b) the EBW scheduler is studied and Fig. 4(a) and (b) depict the results for the SRM scheduler. The average energy efficiency of 57 sectors is plotted in Fig. 3(a) and Fig. 4(a), and the average sum throughput of sectors is depicted in Fig. 3(b) and Fig. 4(b). The proposed algorithm starts at full transmit power and iteratively updates ε and β along the derivative using the update rule in (17). The initial values are chosen as $(\varepsilon_0, \beta_0) = (2, 1)$. It can be observed that both the energy efficiency and throughput increase monotonically per iteration.

Let us first identify the power control gain. In Fig. 3(a), when we compare the power control and no power control cases of the FFR spectrum allocation with EBW scheduler, it can be observed that the energy efficiency of the FFR spectrum allocation increases 2.08 times with the power control. In addition, we observe from Fig. 3(b) that power control brings a 36% throughput increase. Similar gains are observed with the SRM scheduler in Fig. 4(a) and (b) such that the energy efficiency gain is 2.12 times and the throughput gain is 38%. These gains are due to adjusting the downlink transmit power and reducing both the intra- and inter-cell interference in the network. When we evaluate the performance of the algorithm in [7], we observe that it provides negligible gains compared to the case without power control in both metrics. This is due to the fact that the selfish behavior of base stations impairs the network energy efficiency and throughput in an interference dominated region. Notice that in Figs. 3(a), (b) and 4(a), (b) both the power control and no power control curves start almost at the same points and at each iteration we observe the power control curves monotonically increase their values indicating the power control gain.

Second, we analyze the effects of frequency scheduling on the energy efficiency. Comparing Fig. 3(a) and Fig. 4(a), we observe that the energy efficiency of the FFR scheme with the SRM scheduler is 11% better than that of the EBW scheduler. The throughput gain of these two schedulers is similar. This shows that the energy efficiency gain is mostly related to the

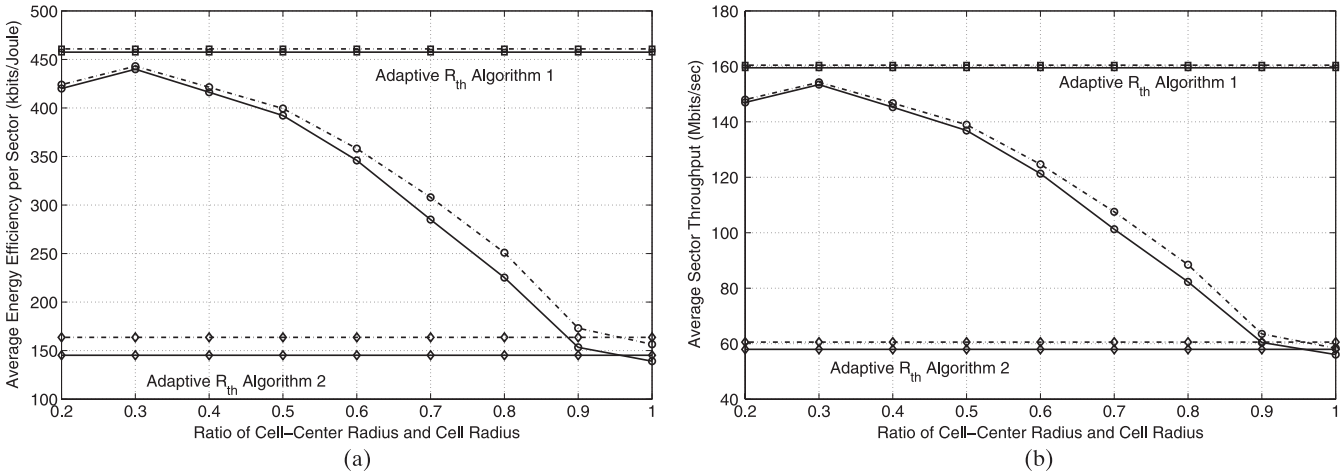

Fig. 5. Average energy efficiency per sector (a) and average sector throughput. (b) versus the ratio of the cell-center region radius to cell radius are depicted for EBW scheduler. Note that dashed lines represent the algorithm with pricing, while the solid lines represent power control only.

throughput gain of the scheduler and the scheduler type has a small effect on the power consumption.

Third, we analyze the performance of spectrum allocation schemes in two-tiers. We observe that employing the EBW scheduler, the fixed FFR scheme outperforms the cochannel allocation by 25% and the orthogonal channel allocation by 59% in terms of energy efficiency. Similar gains are observed in the throughput performance as well. For the SRM scheduler, the cochannel allocation method has 12% and 29% better performance in both metrics compared to the fixed FFR method and orthogonal channel allocation, respectively. This result highlights the importance of the scheduler in use for different spectrum allocations. We note that with power control, FFR performs the best.

Fourth, we compare the FR scheme to the FFR spectrum allocation. We employ the proposed power control method and the SRM scheduler in both cases. As previously mentioned, two types of FR schemes in a two-tier network are investigated. From Fig. 4(a) and (b), we observe that the energy efficiency of FR1 and FR2 are 403 and 262 kbits/Joule, respectively, whereas it is 506 kbits/Joule for the FFR allocation with adaptive cell-center regions. The average sector throughput of FR1, FR2, and FFR spectrum allocations are 142.2, 92.8, and 176.6 Mbits/sec, respectively. These results show that the FFR spectrum allocation provides 26–93% more energy efficient transmissions and 24–90% more throughput per sector compared to the FR spectrum allocation. These results also show that FFR is an effective spectrum allocation method, which effectively utilizes the available spectrum by reducing the interference and increasing the achievable throughput. Similar conclusions can be drawn based on Fig. 3(a) and (b).

Fifth, we study the effects of the cell-center region boundaries. The proposed Adaptive R_{th} Algorithm 1 has similar energy efficiency and throughput performance compared to the fixed radius FFR method with $r_{th} = 0.3R$ in both schedulers. However its performance is significantly higher compared to other constant radii values as depicted in Fig. 5(a) and (b). In addition, it can be expected that Adaptive R_{th} Algorithm 1 significantly outperforms the fixed FFR solution in a dynamic scenario. When compared to the algorithm in [14], Adaptive R_{th} Algorithm 1 outperforms the one in [14] by factors of 2.9 and 2.5 in terms of energy efficiency for the EBW and SRM schedulers, respectively. These gains are due to implementing adaptive cell-center boundaries and better power allocation. Despite the poor performance of Adaptive R_{th} Algorithm 2 in terms of energy efficiency, it provides a fair distribution of resources among MUEs. For example, Jain's fairness index of Adaptive R_{th} Algorithm 2 using the EBW scheduler is 0.5, whereas it is 0.025 with the Adaptive R_{th} Algorithm 1 using the same scheduler.

Finally, we compare the single-tier and two-tier deployments using the FFR scheme with the proposed power control method and the SRM scheduler. From Fig. 4(a) and (b), we observe that the energy efficiency of the single-layer network is 380 bits/Joule and it increases to 506 bits/Joule when picocells are deployed, indicating a 1.3x gain. Moreover, the sector throughput increases from 55 to 175 Mbits/sec from a single-layer to two-tier HetNet deployment, respectively, corresponding to a 3.2x gain. These results demonstrate the substantial gains that can be achieved with the picocell deployment. Again, similar conclusions can be drawn based on Fig. 3(a) and (b), in fact with even larger gains.

Fig. 5(a) shows the average energy efficiency per sector for different cell-center radii using the EBW scheduler. The performance of the proposed adaptive R_{th} algorithms is also presented. We observe that the performance of the FFR system strictly depends on the cell-center region boundaries. When the fixed radius FFR methods are considered and different radii values are enumerated, the system energy efficiency varies between 139 and 439 kbits/Joule. Our simulation results show that the proposed Adaptive R_{th} Algorithm 1 outperforms all other FFR methods in both metrics. On the other hand, Adaptive R_{th} Algorithm 2 performs significantly worse as it prioritizes fairness rather than throughput. Note that there is a 3x gain between the two algorithms in terms of energy efficiency which illustrates the energy efficiency and fairness trade-off.

Fig. 5(b) compares the average sector throughput per sector of the fixed fractional cell-center radii to the adaptive R_{th}

algorithms for the EBW scheduler. Similar to the energy efficiency, throughput performance strictly depends on the cell-center region boundaries such that the average sector throughput varies between 56 and 153 Mbps for different constant cell-center radii values. An important result is that the cell-center radius that maximizes the throughput is the same as that maximizes the energy efficiency. Note that, with another power consumption model, these two radii can take different values.

Fig. 5(a) and (b) also illustrate the effects of the pricing on the energy efficiency and average sector throughput, respectively. Despite the extra information required, the pricing provides only 0.7% and 0.4% improvements in terms of energy efficiency with the Adaptive R_{th} Algorithm 1 using the EBW and SRM schedulers, respectively. The reason for this is as follows. Due to the nature of the FFR method, the inter-cell interference on subbands B, C, and D are significantly suppressed and the pricing method on these bands does not improve the performance of the algorithm remarkably. Note that with the Adaptive R_{th} Algorithm 1, when the number of users in the sector increases, the cell-center radius gets closer to the MeNB, and the inter-cell interference to this user is very limited. On the other hand, we observe that with the Adaptive R_{th} Algorithm 2, pricing provides higher gains. The energy efficiency improvements are 13% and 8% for EBW and SRM schedulers with pricing, respectively. This is due to the fact that since the cell-center radius is closer to cell edge than it is for the Adaptive R_{th} Algorithm 1, the inter-cell interference becomes more critical and the pricing gain is higher.

VI. Conclusion

Energy consumption of a wireless network is a serious concern for the next generation cellular networks. To address this problem, we have proposed an energy-efficient resource allocation algorithm for HetNets with the FFR scheme. The proposed algorithm decouples the frequency and power allocation problems and successively solves each of them. It employs the gradient ascent method to solve the power allocation problem. Based on our simulations, we show that the proposed algorithm significantly improves both the energy efficiency and throughput. We also quantify the individual contributions of the effects of cell-center region, power control, and frequency scheduling gains in order to provide design guidelines. It is demonstrated that the proposed power control algorithm provides the most significant gains, while moderate gains can be achieved with the SRM scheduler and Adaptive R_{th} Algorithm 1. An upper bound based on the interference pricing method is also investigated and the performance gap is shown to be only marginal. Finally, we show that significant energy savings are possible with the proposed algorithm which reduces the operational expenditures for the network operators.

Appendix

In what follows, we prove that $\eta_i(\varepsilon, \beta)$ is quasiconcave in ε and β. It follows from Proposition 2 that $\eta_i(\varepsilon, \beta)$ is a quasiconcave function if and only if the following holds

$$\mathbf{y}^T \nabla \eta_i(\varepsilon, \beta) = 0 \text{ and } \mathbf{y}^T \nabla^2 \eta_i(\varepsilon, \beta) \mathbf{y} \leq 0 \tag{22}$$

where $\mathbf{y} = [y_1 \;\; y_2]^T$. First, we introduce new definitions for the proof, and then express the first and second order derivatives. Let $R_i(\varepsilon, \beta)$ denote the aggregate throughput of sector i as

$$\begin{aligned} R_i(\varepsilon, \beta) = &\sum_{k \in \mathcal{K}_M^C} \sum_{n \in \mathcal{N}_{M_k}^C} R_1^{(k,n)}(\varepsilon, \beta) \\ &+ \sum_{k \in \mathcal{K}_M^X} \sum_{n \in \mathcal{N}_{M_k}^X} R_2^{(k,n)}(\varepsilon, \beta) \\ &+ \sum_{k \in \mathcal{K}_P^X} \sum_{n \in \mathcal{N}_{P_k}^X \cap \mathcal{N}_M^C} R_3^{(k,n)}(\varepsilon, \beta) \end{aligned} \tag{23}$$

where

$$\begin{aligned} R_1^{(k,n)}(\varepsilon, \beta) &= \log\left(1 + \frac{\beta a}{b + \varepsilon c}\right) \\ R_2^{(k,n)}(\varepsilon, \beta) &= \log\left(1 + \frac{\varepsilon \beta d}{b + \varepsilon c}\right) \\ R_3^{(k,n)}(\varepsilon, \beta) &= \log\left(1 + \frac{f}{\frac{\beta g}{b + \varepsilon c} + h}\right) \end{aligned} \tag{24}$$

where $a = P_{\max,M} g_{k,m}^{(n)} / I_k^{(n)}$, $b = N_M^C$, $c = N_M^X$, $d = P_{\max,M} g_{k,m}^{(n)} / (N_0 \Delta f)$, $f = P_{\max,P} / N_P^X g_{l,p}^{(n)}$, $g = P_{\max,M} g_{k,m}^{(n)}$, and $h = N_0 \Delta f$. Due to space considerations, we denote $R_i(\varepsilon, \beta)$, $R_1^{(k,n)}(\varepsilon, \beta)$, $R_2^{(k,n)}(\varepsilon, \beta)$, and $R_2^{(k,n)}(\varepsilon, \beta)$ by $R_i, R_1^{(k,n)}, R_3^{(k,n)}$, and $R_3^{(k,n)}$, respectively. Using these definitions, the first derivative of R_i with respect to ε can be expressed as

$$\begin{aligned} \frac{\partial R_i}{\partial \varepsilon} = &\sum_{k \in \mathcal{K}_M^C} \sum_{n \in \mathcal{N}_{M_k}^C} \frac{\partial R_1^{(k,n)}}{\partial \varepsilon} + \sum_{k \in \mathcal{K}_M^X} \sum_{n \in \mathcal{N}_{M_k}^X} \frac{\partial R_2^{(k,n)}}{\partial \varepsilon} \\ &+ \sum_{k \in \mathcal{K}_P^X} \sum_{n \in \mathcal{N}_{P_k}^X \cap \mathcal{N}_M^C} \frac{\partial R_3^{(k,n)}}{\partial \varepsilon} \end{aligned} \tag{25}$$

where

$$\begin{aligned} \frac{\partial R_1^{(k,n)}}{\partial \varepsilon} &= -\frac{ac\beta}{(b + c\varepsilon)(a\beta + b + c\varepsilon)} \\ \frac{\partial R_2^{(k,n)}}{\partial \varepsilon} &= \frac{bd\beta}{(b + c\varepsilon)\,(b + \varepsilon(c + d\beta))} \\ \frac{\partial R_3^{(k,n)}}{\partial \varepsilon} &= \frac{cfg\beta}{(h(b + c\varepsilon) + g\beta)\,((f + h)(b + c\varepsilon) + g\beta)}. \end{aligned} \tag{26}$$

The second derivative of R_i with respect to ε is given by

$$\begin{aligned} \frac{\partial^2 R_i}{\partial \varepsilon^2} = &\sum_{k \in \mathcal{K}_M^C} \sum_{n \in \mathcal{N}_{M_k}^C} \frac{\partial^2 R_1^{(k,n)}}{\partial \varepsilon^2} + \sum_{k \in \mathcal{K}_M^X} \sum_{n \in \mathcal{N}_{M_k}^X} \frac{\partial^2 R_2^{(k,n)}}{\partial \varepsilon^2} \\ &+ \sum_{k \in \mathcal{K}_P^X} \sum_{n \in \mathcal{N}_{P_k}^X \cap \mathcal{N}_M^C} \frac{\partial^2 R_3^{(k,n)}}{\partial \varepsilon^2} \end{aligned} \tag{27}$$

where

$$\frac{\partial^2 R_1^{(k,n)}}{\partial \varepsilon^2} = \frac{\beta a c^2 \left(a\beta + 2(b + c\varepsilon)\right)}{(b + c\varepsilon)^2 (a\beta + b + c\varepsilon)^2}$$
$$\frac{\partial^2 R_2^{(k,n)}}{\partial \varepsilon^2} = -\frac{bd\beta \left((b + c\varepsilon)(2c + d\beta) + cd\varepsilon\beta\right)}{(b + c\varepsilon)^2 \left(b + \varepsilon(c + d\beta)\right)^2}$$
$$\frac{\partial^2 R_3^{(k,n)}}{\partial \varepsilon^2} = -\frac{c^2 fg\beta \left(2h(f + h)(b + c\varepsilon) + g\beta(f + 2h)\right)}{\left(h(b + c\varepsilon) + g\beta\right)^2 \left((f + h)(b + c\varepsilon) + g\beta\right)^2}. \tag{28}$$

Similarly, the first derivative of R_i with respect to β is

$$\frac{\partial R_i}{\partial \beta} = \sum_{k \in \mathcal{K}_M^C} \sum_{n \in \mathcal{N}_{M_k}^C} \frac{\partial R_1^{(k,n)}}{\partial \beta} + \sum_{k \in \mathcal{K}_M^X} \sum_{n \in \mathcal{N}_{M_k}^X} \frac{\partial R_2^{(k,n)}}{\partial \beta} + \sum_{k \in \mathcal{K}_P^X} \sum_{n \in \mathcal{N}_{P_k}^X \cap \mathcal{N}_M^C} \frac{\partial R_3^{(k,n)}}{\partial \beta} \tag{29}$$

where

$$\frac{\partial R_1^{(k,n)}}{\partial \beta} = \frac{a}{a\beta + b + c\varepsilon}, \frac{\partial R_2^{(k,n)}}{\partial \beta} = \frac{d\varepsilon}{b + \varepsilon\,(c + d\beta)}$$
$$\frac{\partial R_3^{(k,n)}}{\partial \beta} = -\frac{fg(b + c\varepsilon)}{\left(h(b + c\varepsilon) + g\beta\right)\left((f + h)(b + c\varepsilon) + g\beta\right)}. \tag{30}$$

The second derivative of R_i with respect to β is given by

$$\frac{\partial^2 R_i}{\partial \beta^2} = \sum_{k \in \mathcal{K}_M^C} \sum_{n \in \mathcal{N}_{M_k}^C} \frac{\partial^2 R_1^{(k,n)}}{\partial \beta^2} + \sum_{k \in \mathcal{K}_M^X} \sum_{n \in \mathcal{N}_{M_k}^X} \frac{\partial^2 R_2^{(k,n)}}{\partial \beta^2} + \sum_{k \in \mathcal{K}_P^X} \sum_{n \in \mathcal{N}_{P_k}^X \cap \mathcal{N}_M^C} \frac{\partial^2 R_3^{(k,n)}}{\partial \beta^2} \tag{31}$$

where

$$\frac{\partial^2 R_1^{(k,n)}}{\partial \beta^2} = -\frac{a^2}{(a\beta + b + c\varepsilon)^2},$$
$$\frac{\partial^2 R_2^{(k,n)}}{\partial \beta^2} = -\frac{d^2\varepsilon^2}{\left(b + \varepsilon(c + d\beta)\right)^2}$$
$$\frac{\partial^2 R_3^{(k,n)}}{\partial \beta^2} = \frac{fg^2(b + c\varepsilon)\left((f + 2h)(b + c\varepsilon) + 2g\beta\right)}{\left(h(b + c\varepsilon) + g\beta\right)^2 \left((f + h)(b + c\varepsilon) + g\beta\right)^2}. \tag{32}$$

The derivative of R_i with respect to ε and β is

$$\frac{\partial^2 R_i}{\partial \varepsilon \partial \beta} = \sum_{k \in \mathcal{K}_M^C} \sum_{n \in \mathcal{N}_{M_k}^C} \frac{\partial^2 R_1^{(k,n)}}{\partial \varepsilon \partial \beta} + \sum_{k \in \mathcal{K}_M^X} \sum_{n \in \mathcal{N}_{M_k}^X} \frac{\partial^2 R_2^{(k,n)}}{\partial \varepsilon \partial \beta} + \sum_{k \in \mathcal{K}_P^X} \sum_{n \in \mathcal{N}_{P_k}^X \cap \mathcal{N}_M^C} \frac{\partial^2 R_3^{(k,n)}}{\partial \varepsilon \partial \beta} \tag{33}$$

where

$$\frac{\partial^2 R_1^{(k,n)}}{\partial \varepsilon \partial \beta} = -\frac{ac}{(a\beta + b + c\varepsilon)^2}$$
$$\frac{\partial^2 R_2^{(k,n)}}{\partial \varepsilon \partial \beta} = \frac{bd}{\left(b + \varepsilon(c + d\beta)\right)^2}$$
$$\frac{\partial^2 R_3^{(k,n)}}{\partial \varepsilon \partial \beta} = \frac{cfg\left((f + h)h(b + c\varepsilon)^2 - g^2\beta^2\right)}{\left(h(b + c\varepsilon) + g\beta\right)^2 \left((f + h)(b + c\varepsilon) + g\beta\right)^2}. \tag{34}$$

The gradient of $\eta(\varepsilon, \beta)$ can be expressed as

$$\nabla \eta(\varepsilon, \beta) = \begin{pmatrix} \frac{\partial \eta(\varepsilon,\beta)}{\partial \varepsilon} \\ \frac{\partial \eta(\varepsilon,\beta)}{\partial \beta} \end{pmatrix} = \begin{pmatrix} \frac{\partial R_i}{\partial \varepsilon}\frac{1}{\psi} \\ \frac{\partial R_i}{\partial \beta}\frac{1}{\psi} - \frac{R_i}{\psi^2}\frac{\partial \psi}{\partial \beta} \end{pmatrix} \tag{35}$$

where $(\partial R_i/\partial \varepsilon) = (\partial R_1/\partial \varepsilon) + (\partial R_2/\partial \varepsilon) + (\partial R_3/\partial \varepsilon)$ and $(\partial R_i/\partial \beta) = (\partial R_1/\partial \beta) + (\partial R_2/\partial \beta) + (\partial R_3/\partial \beta)$.

Consider that $y^T \nabla \eta_i = 0$ is satisfied and use (35) to rearrange terms, we have $(\partial R_i/\partial \varepsilon)y_1 + (\partial R_i/\partial \beta)y_2 = 1/\psi(\partial \psi/\partial \beta)R_i y_2$. The Hessian of η_i is given by

$$\nabla^2 \eta(\varepsilon, \beta) = \frac{1}{\psi} \begin{pmatrix} \frac{\partial^2 R_i}{\partial \varepsilon^2} & \frac{\partial^2 R_i}{\partial \varepsilon \partial \beta} - \frac{\partial R_i}{\partial \varepsilon}\frac{\frac{\partial \psi}{\partial \beta}}{\psi} \\ \frac{\partial^2 R_i}{\partial \varepsilon \partial \beta} - \frac{\partial R_i}{\partial \varepsilon}\frac{\frac{\partial \psi}{\partial \beta}}{\psi} & \Phi \end{pmatrix} \tag{36}$$

where

$$\Phi = \frac{\partial^2 R_i}{\partial \beta^2} - \frac{2}{\psi}\frac{\partial R_i}{\partial \beta}\frac{\partial \psi}{\partial \beta} - R_i\frac{\left(\frac{\partial^2 \psi}{\partial \beta^2}\right)^2}{\psi} + 2R_i\frac{\left(\frac{\partial \psi}{\partial \beta}\right)^2}{\psi^2}. \tag{37}$$

For the power consumption model in (11), $\frac{\partial^2 \psi}{\partial \beta^2} = 0$. When we expand the terms, we get

$$\mathbf{y}^T \nabla^2 \eta_i(\varepsilon, \beta)\mathbf{y} = \frac{\partial^2 R_i}{\partial \varepsilon^2} y_1^2 + 2\left(\frac{\partial^2 R_i}{\partial \varepsilon \partial \beta} - \frac{\partial R_i}{\partial \varepsilon}\frac{\frac{\partial \psi}{\partial \beta}}{\psi}\right) y_1 y_2 + \Phi y_2^2. \tag{38}$$

Substituting the condition $y^T \nabla \eta_i = 0$ in (38) and rearranging terms, we have

$$\mathbf{y}^T \nabla^2 \eta_i \mathbf{y} = \frac{1}{\psi}\left(\frac{\partial^2 R_i}{\partial \varepsilon^2} y_1^2 + 2\frac{\partial^2 R_i}{\partial \varepsilon \partial \beta} y_1 y_2 + \frac{\partial^2 R_i}{\partial \beta^2} y_2^2\right)$$
$$= \frac{1}{\psi}\mathbf{y}^T \nabla^2 R_i\, \mathbf{y}. \tag{39}$$

where $\nabla^2 R_i$ denotes the Hessian of R_i. This means that η_i is quasiconcave if and only if R_i is quasiconcave. Next, we

analyze the quasiconcavity of R_i. Using in (28), (32), and (34) in (39) to obtain $\mathbf{y}^T\nabla^2 R_i\mathbf{y} \leq 0$, we need to show that

$$\sum_{k\in\mathcal{K}_M^C}\sum_{n\in\mathcal{N}_{M_k}^C}\left(\frac{\partial^2 R_1^{(n)}}{\partial\varepsilon^2}y_1^2+2\frac{\partial^2 R_1^{(n)}}{\partial\varepsilon\partial\beta}y_1y_2+\frac{\partial^2 R_1^{(n)}}{\partial\beta^2}y_2^2\right)+\sum_{k\in\mathcal{K}_M^X}\sum_{n\in\mathcal{N}_{M_k}^X}\left(\frac{\partial^2 R_2^{(n)}}{\partial\varepsilon^2}y_1^2+2\frac{\partial^2 R_2^{(n)}}{\partial\varepsilon\partial\beta}y_1y_2+\frac{\partial^2 R_2^{(n)}}{\partial\beta^2}y_2^2\right)+\sum_{k\in\mathcal{K}_P^X}\sum_{n\in\mathcal{N}_{P_k}^X\cap\mathcal{N}_M^C}\left(\frac{\partial^2 R_3^{(n)}}{\partial\varepsilon^2}y_1^2+2\frac{\partial^2 R_3^{(n)}}{\partial\varepsilon\partial\beta}y_1y_2+\frac{\partial^2 R_3^{(n)}}{\partial\beta^2}y_2^2\right)\leq 0. \tag{40}$$

Notice that the summations in (40) are grouped into subcarriers based on their locations within the cell. The contributions of the cell-center and cell-edge MUEs are captured in the first two summations in (40), while the third is of the cell-edge PUEs. For the proof, it is necessary to show that the sum of these summations is non-positive.

First, we identify the condition for the first summation in (40), that is the terms for the cell-center MUEs, as

$$\frac{\beta ac^2\left(a\beta+2(b+c\varepsilon)\right)}{(b+c\varepsilon)^2}y_1^2-2acy_1y_2-a^2y_2^2\leq 0. \tag{41}$$

Notice that this is the condition that relates to the cell-center MUEs.

Next, we investigate the condition for the second summation in (40) to hold, that is

$$-\frac{bd\beta\left((b+c\varepsilon)(2c+d\beta)+cd\varepsilon\beta\right)}{(b+c\varepsilon)^2}y_1^2+2bdy_1y_2-d^2\varepsilon^2y_2^2\leq 0 \tag{42}$$

When we rearrange terms, we have the necessary condition for the cell-edge MUEs such as

$$2bd(b+c\varepsilon)^2y_1y_2\leq bd\beta\left((b+c\varepsilon)(2c+d\beta)+cd\varepsilon\beta\right)y_1^2+d^2\varepsilon^2(b+c\varepsilon)^2y_2^2. \tag{43}$$

Finally, we see that the condition for the cell-edge PUEs is

$$-c^2fg\beta\left(2h(f+h)(b+c\varepsilon)+g\beta(f+2h)\right)y_1^2+2cfg\left((f+h)h(b+c\varepsilon)^2-g^2\beta^2\right)y_1y_2+fg^2(b+c\varepsilon)\left((f+2h)(b+c\varepsilon)+2g\beta\right)y_2^2\leq 0. \tag{44}$$

In our extensive simulations, we have observed that (41)–(44) are always satisfied. This makes us conjecture that R_i and η_i are negative semi-definite, as we have observed numerically. Therefore, we conclude that the function η_i should be quasi-concave in ε and β.

REFERENCES

[1] K. Davaslioglu and E. Ayanoglu, "Quantifying potential energy efficiency gain in green cellular wireless networks," *IEEE Commun. Surveys Tuts.*, vol. 16, no. 4, pp. 2065–2091, 4th Quart. 2014.

[2] H. Holma and A. Toskala, *LTE-Advanced: 3GPP Solution for IMT-Advanced*. West Sussex, U.K.: Wiley, 2012.

[3] C. Han *et al.*, "Green radio: Radio techniques to enable energy-efficient wireless networks," *IEEE Commun. Mag*, vol. 49, no. 6, pp. 46–54, Jun. 2011.

[4] E. Hossain, V. K. Bhargava, and G. P. Fettweis, *Green Radio Communication Networks*. Cambridge, U.K.: Cambridge Univ. Press, 2012.

[5] J. Wu, S. Rangan, and H. Zhang, *Green Communications: Theoretical Fundamentals, Algorithms and Applications*. Boca Raton, FL, USA: CRC Press, 2013.

[6] L. Hoo, B. Halder, J. Tellado, and J. Cioffi, "Multiuser transmit optimization for multicarrier broadcast channels: Asymptotic FDMA capacity region and algorithms," *IEEE Trans. Commun.*, vol. 52, no. 6, pp. 922–930, Jun. 2004.

[7] W. Yu and J. Cioffi, "On constant power water-filling," in *Proc. IEEE ICC*, Jun. 2001, vol. 6, pp. 1665–1669.

[8] G. Miao, N. Himayat, and G. Li, "Energy-efficient link adaptation in frequency-selective channels," *IEEE Trans. Commun.*, vol. 58, no. 2, pp. 545–554, Feb. 2010.

[9] G. Miao, N. Himayat, G. Li, and S. Talwar, "Distributed interference-aware energy-efficient power optimization," *IEEE Trans. Wireless Commun.*, vol. 10, no. 4, pp. 1323–1333, Apr. 2011.

[10] C. Xiong, G. Li, S. Zhang, Y. Chen, and S. Xu, "Energy- and spectral-efficiency tradeoff in downlink OFDMA networks," *IEEE Trans. Wireless Commun.*, vol. 10, no. 11, pp. 3874–3886, Nov. 2011.

[11] T. Novlan, R. Ganti, A. Ghosh, and J. Andrews, "Analytical evaluation of fractional frequency reuse for heterogeneous cellular networks," *IEEE Trans. Commun.*, vol. 60, no. 7, pp. 2029–2039, Jul. 2012.

[12] Z. Xu, G. Li, C. Yang, and X. Zhu, "Throughput and optimal threshold for FFR schemes in OFDMA cellular networks," *IEEE Trans. Wireless Commun.*, vol. 11, no. 8, pp. 2776–2785, Aug. 2012.

[13] M. Assaad, "Optimal fractional frequency reuse (FFR) in multicellular OFDMA system," in *Proc. IEEE VTC Fall*, Sep. 2008, pp. 1–5.

[14] N. Saquib, E. Hossain, and D. I. Kim, "Fractional frequency reuse for interference management in LTE-advanced HetNets," *IEEE Wireless Commun.*, vol. 20, no. 2, pp. 113–122, Apr. 2013.

[15] T. Lee, J. Yoon, S. Lee, and J. Shin, "Interference management in OFDMA femtocell systems using fractional frequency reuse," in *Proc. ICCCAS*, Jul. 2010, pp. 176–180.

[16] P. Lee, T. Lee, J. Jeong, and J. Shin, "Interference management in LTE femtocell systems using fractional frequency reuse," in *Proc. ICACT*, Feb. 2010, vol. 2, pp. 1047–1051.

[17] K. Davaslioglu and E. Ayanoglu, "Efficiency and fairness trade-offs in SC-FDMA schedulers," *IEEE Trans. Wireless Commun.*, vol. 13, no. 6, pp. 2991–3002, Jun. 2014.

[18] D. Schmidt, C. Shi, R. Berry, M. Honig, and W. Utschick, "Distributed resource allocation schemes," *IEEE Signal Process. Mag.*, vol. 26, no. 5, pp. 53–63, Sep. 2009.

[19] J. Huang, R. Berry, and M. Honig, "Distributed interference compensation for wireless networks," *IEEE J. Sel. Areas Commun.*, vol. 24, no. 5, pp. 1074–1084, May 2006.

[20] C. Shi, R. Berry, and M. Honig, "Monotonic convergence of distributed interference pricing in wireless networks," in *Proc. IEEE ISIT*, Jun. 2009, pp. 1619–1623.

[21] C. Saraydar, N. B. Mandayam, and D. Goodman, "Pricing and power control in a multicell wireless data network," *IEEE J. Sel. Areas Commun.*, vol. 19, no. 10, pp. 1883–1892, Oct. 2001.

[22] C. Saraydar, N. B. Mandayam, and D. Goodman, "Efficient power control via pricing in wireless data networks," *IEEE Trans. Commun.*, vol. 50, no. 2, pp. 291–303, Feb. 2002.

[23] C. Gizelis and D. Vergados, "A survey of pricing schemes in wireless networks," *IEEE Commun. Surveys Tuts.*, vol. 13, no. 1, pp. 126–145, 1st Quart. 2011.

[24] P. Marsch and G. P. Fettweis, *Coordinated Multi-Point in Mobile Communications: From Theory to Practice*. Cambridge, U.K.: Cambridge Univ. Press, 2011.

[25] G. Auer *et al.*, "How much energy is needed to run a wireless network?" *IEEE Wireless Commun.*, vol. 18, no. 5, pp. 40–49, Oct. 2011.

[26] F. Richter, A. Fehske, and G. Fettweis, "Energy efficiency aspects of base station deployment strategies for cellular networks," in *Proc. IEEE Veh. Technol. Conf. Fall*, Sep. 2009, pp. 1–5.

[27] H. Holtkamp, G. Auer, V. Giannini, and H. Haas, "A parameterized base station power model," *IEEE Commun. Lett.*, vol. 17, no. 11, pp. 2033–2035, Nov. 2013.

[28] Q. Li, R. Hu, Y. Xu, and Y. Qian, "Optimal fractional frequency reuse and power control in the heterogeneous wireless networks," *IEEE Trans. Wireless Commun.*, vol. 12, no. 6, pp. 2658–2668, Jun. 2013.

[29] A. Najjar, N. Hamdi, and A. Bouallegue, "Efficient frequency reuse scheme for multi-cell OFDMA systems," in *Proc. IEEE ISCC*, Jul. 2009, pp. 261–265.

[30] *Further Advancements for E-UTRA Physical Layer Aspects (Release 9)*, 3GPP, TR 36.814, Mar. 2010.
[31] D. P. Bertsekas, *Nonlinear Programming*. Belmont, MA, USA: Athena Scientific, 1995.
[32] E. Wolfstetter, *Topics in Microeconomics: Industrial Organization, Auctions, and Incentives*. New York, NY, USA: Cambridge Univ. Press, 2003.
[33] K. Davaslioglu and E. Ayanoglu, "Interference-based cell selection in heterogeneous networks," in *Proc. ITA Workshop*, San Diego, CA, USA, Feb. 2013, pp. 1–6.

Kemal Davaslioglu (S'06) received the B.S. degree from Bilkent University, Ankara, Turkey, in 2008 and the M.S. degree from Bogazici University, Istanbul, Turkey, in 2010, both in electrical engineering. He is currently pursuing the Ph.D. degree in the Department of Electrical Engineering and Computer Science, University of California, Irvine, CA, USA, where he is affiliated with the Center for Pervasive Communications and Computing. From 2011 to 2012, he was with Broadcom Corp., Irvine, working on 10-Gigabit Ethernet systems. His research interests include resource allocation, load balancing, and energy-efficiency in next-generation mobile wireless networks, wireless communication theory, signal processing for wireless communications, and ultra-wideband communications.

Cemil Can Coskun (S'07) received the bachelor's degree and master degree in electrical and electronics engineering from Bilkent University, Turkey, in 2010 and 2012, respectively. He is currently a Ph.D. student in the Department of Electrical Engineering and Computer Science, University of California, Irvine. His research interests are in the area of green communications and the wireless networks.

Ender Ayanoglu (S'82–M'85–SM'90–F'98) received the M.S. and Ph.D. degrees in electrical engineering from Stanford University, Stanford, CA, USA, in 1982 and 1986, respectively. He was with the Communications Systems Research Laboratory, part of AT&T Bell Laboratories, Holmdel, NJ, USA, until 1996, and Bell Labs, Lucent Technologies until 1999. From 1999 until 2002, he was a Systems Architect at Cisco Systems, Inc., San Jose, CA. Since 2002, he has been a Professor in the Department of Electrical Engineering and Computer Science, University of California, Irvine, CA, where he served as the Director of the Center for Pervasive Communications and Computing and held the Conexant-Broadcom Endowed Chair during 2002–2010.

His past accomplishments include invention of the 56K modems, characterization of wavelength conversion gain in Wavelength Division Multiplexed (WDM) systems, and diversity coding, a technique for link failure recovery in communication networks employing erasure coding in 1990, prior to the publication of the first papers on network coding. During 2000–2001, he served as the founding chair of the IEEE-ISTO Broadband Wireless Internet Forum (BWIF), an industry standards organization which developed and built a broadband wireless system employing Orthogonal Frequency Division Multiplexing (OFDM) and a Medium Access Control (MAC) algorithm that provides Quality-of-Service (QoS) guarantees. This system is the precursor of today's Fourth Generation (4G) cellular wireless systems such as WiMAX, LTE, and LTE-Advanced.

From 1993 until 2014, he was an Editor, and since January 2014 is a Senior Editor of the IEEE TRANSACTIONS ON COMMUNICATIONS. He served as the Editor-in-Chief of the IEEE TRANSACTIONS ON COMMUNICATIONS from 2004 to 2008. Currently, he is serving as the Editor-in-Chief of the IEEE JOURNAL ON SELECTED AREAS IN COMMUNICATIONS—Series on Green Communications and Networking. From 1990 to 2002, he served on the Executive Committee of the IEEE Communications Society Communication Theory Committee, and from 1999 to 2001, was its Chair. He is the recipient of the IEEE Communications Society Stephen O. Rice Prize Paper Award in 1995 and the IEEE Communications Society Best Tutorial Paper Award in 1997. He received the Outstanding Service Award from the IEEE Communications Society Communication Theory Technical Committee in 2014.